



## AN ENHANCED DISPLACEMENT-BASED ELEMENT TO ACCOUNT FOR TENSION SHIFT EFFECTS

D. Tarquini<sup>(1)</sup>, J.P. Almeida<sup>(2)</sup>, K. Beyer<sup>(3)</sup>

<sup>(1)</sup> PhD candidate, Earthquake Engineering and Structural Dynamics Laboratory (EESD), School of Architectural, Civil and Environmental Engineering (ENAC), École Polytechnique Fédérale de Lausanne (EPFL), Switzerland, [danilo.tarquini@epfl.ch](mailto:danilo.tarquini@epfl.ch)

<sup>(2)</sup> Post-doctoral Researcher, Earthquake Engineering and Structural Dynamics Laboratory (EESD), School of Architectural, Civil and Environmental Engineering (ENAC), École Polytechnique Fédérale de Lausanne (EPFL), Switzerland, [joao.almeida@epfl.ch](mailto:joao.almeida@epfl.ch)

<sup>(3)</sup> Assistant Professor, Earthquake Engineering and Structural Dynamics Laboratory (EESD), School of Architectural, Civil and Environmental Engineering (ENAC), École Polytechnique Fédérale de Lausanne (EPFL), Switzerland, [katrin.beyer@epfl.ch](mailto:katrin.beyer@epfl.ch)

### Abstract

Engineers and researchers often use nonlinear beam-column elements to simulate the response of reinforced concrete structures. Namely, distributed plasticity elements are arguably the most attractive due to the good compromise between accuracy and computational time. Formulation wise, three types of distributed plasticity beam elements can be distinguished: displacement-based, force-based and mixed formulations. The simplicity of numerical implementation renders the first class of elements particularly appealing from a practical point of view despite the fact that the classically employed shape functions yield exact solutions only for linear elastic problems and nodal loads. As a consequence, when material or geometrical nonlinearities are involved, equilibrium within the element is not strictly satisfied.

Recent experimental tests on the inelastic behavior of bridge piers have shown that the curvature profile above the base section of a fixed structural member is different from the one simulated by a plane-section force-based beam formulation, which satisfies exact equilibrium and considers only the effect of the moment gradient. These tests confirmed in particular that the tension shift effects due to inclined cracks in concrete members are responsible for a curvature distribution that evolves in a bilinear shape along the member height during the inelastic phase of the response. This paper presents an enhanced displacement-based element strictly verifying axial equilibrium which ensures the axial force to remain constant within the element while maintaining the linearity of the curvature profile. This yields in two advantages over the classical displacement-based element: First, it yields a better prediction of the moment capacity as the axial force verifies equilibrium exactly, which is not the case in classical displacement-based elements where only an average equilibrium is guaranteed. Second, the combination between the axial force equilibrium and the linear curvature profile can be used to simulate the effects of tension shift in RC elements, both at the global and local level.

The new element is first applied to an example column to illustrate its main features, and then used to simulate the response of a reinforced concrete bridge pier that was tested under cyclic loading. By comparing numerical to experimental results, it is shown that the proposed element predicts satisfactorily the global force-displacement response. Additionally, when compared to simulations using classical displacement-based or force-based beam elements, a greater accuracy can be obtained for the prediction of the evolution of curvatures and rebar strains over the height of the bridge pier for increasing ductility demands. The improved predictions come at the cost of a more involved state determination with respect to the classical displacement-based formulation.

**Keywords:** Beam element; Axial equilibrium; Displacement-based formulation; Distributed inelasticity; Tension shift effects.

## 1. Introduction

Performance Based Earthquake Engineering (PBEE) requires a reliable assessment of structural behaviour under seismic excitation. Nonlinear analysis provides the means for calculating the structural response beyond the elastic range and assessing the expected level of damage.

For reinforced concrete (RC) structures, a commonly employed tool for the simulation of the nonlinear response is represented by beam element models, as they feature an attractive compromise between accuracy and computational cost. Amongst beam formulations, lumped and distributed plasticity approaches can be distinguished. The former, as the name suggests, concentrate the occurrence of inelastic deformations in pre-defined locations along the element length. On the other hand, distributed plasticity elements do not impose *a priori* a specific location for the development of plasticity nor restraints to its progression along the member length. Such type of formulations discretize the element into several numerical integration sections from which the element response is obtained. Each section is typically subdivided into fibres to which an inelastic material constitutive law is assigned.

Within distributed plasticity elements, the choice of the imposed independent fields yields the so-called displacement-based (DB) and force-based (FB) formulations [1]. An important point, in the context of the present work and as further discussed below, is that most of these approaches have been developed for Euler-Bernoulli beam theory (plane sections remain plane and perpendicular to the deformed element axis), which is the beam theory that is available in roughly all the commonly used structural analysis software (e.g., [2,3]). DB formulations employ linear and Hermitian polynomial functions for the axial and transversal displacement fields respectively, which provides an exact solution only for the case of linear elastic material and nodal loads. FB formulations, on the other hand, use constant and linear shape functions for the axial force and bending moment respectively, which results in an exact solution regardless of the material nonlinearity assigned to the fibres. Therefore, one FB element usually suffices to simulate the nonlinear response of a structural member while, if DB elements are used, member discretization in several finite elements is required. Additionally, equilibrium in FB formulations is verified pointwise along the element length whereas in DB elements only the average of the internal forces is in equilibrium with the nodal forces (i.e., equilibrium is only verified in an average sense) [4].

Despite the undebatable superiority of FB elements over the DB counterpart in terms of theoretical accuracy, DB elements are more straightforward and less computationally burdensome for what concerns their formulation and numerical implementation in finite element codes. In fact, unlike for FB elements, no residual sectional strains are transferred to the element level, which allows to forthwith derive the element forces and tangent stiffness matrix by integration of the sectional responses for every increment of element displacements.

In the present work it is postulated that DB formulations, which have been gradually replaced by FB approaches over the past 15-20 years, have good reasons to be revived as they offer a bypass around some of the limitations that stem from the application of the well-known Euler-Bernoulli hypothesis. In fact, the latter has been shown to be quite constraining when compared against experimental evidence of nonlinearly responding RC members. As pointed out by Priestley et al. [5], the first reason for the mismatch between the force-displacement response as obtained from a FB element (which verifies equilibrium in an exact form) and experimental results is the fact that tension shift effects are ignored. The latter cause a linear distribution of plastic curvatures inside the plastic zone of the structural member ([6–9], see Fig. 1). Furthermore, a recent test campaign on circular bridge piers [10] has shown that the intersection of this plastic curvature profile with the elastic curvatures occurs at an increasing height for larger ductility demands (see again Fig. 1). The two above physical phenomena can be analytically simulated by imposing appropriate lateral displacement profiles to the beam finite element formulation (in accordance with the observed linear curvature profiles in the plastic hinge region), suggesting that DB approaches and not FB formulations are the natural framework to develop such finite element. This paper represents a first step to address these issues and hence to gradually reflect experimental findings in beam formulations that can later be used to predict the performance of RC structures more confidently in engineering practice.

To accomplish such goal, one fundamental drawback of the classical DB formulations should be addressed beforehand. As mentioned above, the imposed linear axial displacement field implies that equilibrium is only verified in an average sense which, in case of material nonlinearity, results in different values of the axial force for distinct integration sections. This leads to a misevaluation of the moment capacity of the structural member and therefore to a poor local and global performance of the finite element [4]. This paper presents an enhanced DB element in which the axial equilibrium is strictly verified (hence emulating the advantages of a FB formulation in this respect) through the use of adaptive shape functions for the generalized axial strains. This formulation will be further extended in the future to include transversal displacement profiles that simulate the above mentioned effects of tension shift on the bilinearity of the curvature profile along the element and corresponding evolution with ductility demand.

The new element and its state determination are described in Section 2. Section 3 presents an application example showing the comparison between the new element and the classical DB and FB formulations, whilst in Section 4 the proposed DB element is validated against experimental results. Future developments and conclusions are provided in Section 5.

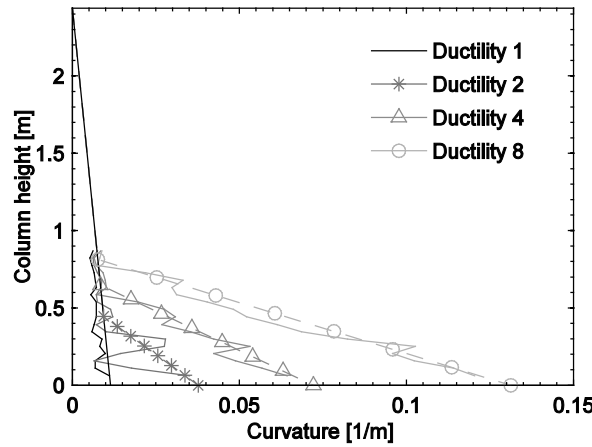


Fig. 1 – Experimental curvature profile and line of best fit for a circular cantilever pier subjected to different levels of imposed displacement ductility (adapted from [9]).

## 2. Axially Equilibrated Displacement-based element: State Determination

The concept of a displacement-based element satisfying axial equilibrium was originally proposed by Izzudin et al. [11] for the case of nonlinear-elastic problems. A quartic formulation was used for the lateral displacement field while no shape functions were defined for the axial displacement field. The present formulation, which employs Hermitian polynomials for the lateral displacement field, uses the same procedure described in [11] to achieve axial equilibrium. However, a variational approach is applied to determine the element end forces and the tangent stiffness matrix which yields to differences, with regards to [11], in the evaluation of the derivatives of the axial load with respect to the basic displacements. A full discussion on the mathematical background of the proposed DB element is not provided due to space limitations. Instead, the main aspects concerning the element state determination are described in the following paragraphs.

The state determination of the enhanced displacement-based element satisfying axial equilibrium is schematically illustrated in the flowchart of Fig. 2. It consists in determining the element basic forces and tangent stiffness matrix given a set of incremental basic displacements. The element forces  $\mathbf{p}_{bsc}$  and displacements  $\mathbf{u}_{bsc}$  acting on the element in the basic reference system (e.g. without rigid body modes) include the nodal axial force/bending moments ( $P_1, M_1, M_2$ ) and the end axial displacement/rotations ( $U_1, \theta_1, \theta_2$ ) respectively. The steps to be performed to connect the basic and the global reference systems involve classical

structural analysis operations (e.g. the use of rotation matrix and nonlinear compatibility and equilibrium relations, such as those associated to a corotational formulation) and will thus be omitted.

In the classical DB formulations, a linear shape function for the axial displacement field  $u(x)$ —i.e. corresponding to a constant average axial strain profile  $\varepsilon_0(x)$ —is employed along the element. Hermitian polynomials are used instead for the transverse displacement field  $v(x)$  resulting in a linear curvature profile  $\kappa(x)$ . When nonlinear material behaviour is considered, such generalized deformations lead to generalized sectional forces— $N(x)$ ,  $M(x)$ —which are not strictly equilibrated, but only on an average sense.

Straightforward equilibrium considerations imply that, when no distributed axial loads are applied along the element axis, the axial force at the integration section  $j N(x_{IPj})$  has to be the same in all integration sections of the element and equal to the basic axial force  $P_1$ . The former condition, combined with the fact that the integral (along the element length) of the average axial strain  $\varepsilon_0(x_{IPj})$  must be equal to the applied axial displacement  $U_1$ , can be manipulated to provide direct relationships between  $\Delta\varepsilon_0(x_{IPj})$  and the current generalized axial force  $N(x_{IPj})$  at each integration section (IP) of coordinates  $x_{IPj}$  [11]. An iterative procedure that systematically adjusts the values of the incremental axial strains  $\Delta\varepsilon_0(x_{IPj})$  can therefore be set up until the difference between the generalized axial forces  $N(x_{IPj})$  in all the integration sections is below a defined tolerance [11]. Once convergence is attained, the set of axial strains  $\varepsilon_0(x_{IPj})$  strictly satisfying axial equilibrium is known and the derivatives of the generalized strains with respect to the basic displacement vector  $\partial\varepsilon_0(x_{IPj}) / \partial\mathbf{u}_{bsc}$  can be updated. The principle of virtual work is then applied in order to determine the set of equilibrated element basic forces  $\mathbf{p}_{bsc}$  as well as a consistent element tangent basic stiffness matrix  $\mathbf{K}_T$ .

### 3. Axially Equilibrated DB vs Classical Euler-Bernoulli Beam Formulations

The axially equilibrated displacement-based formulation has been implemented in the finite element software *SAGRES* (*Software for Analysis of GRadient Effects in Structures*), originally developed by the second author. In the following an application example compares the results (both at the global and local level) of the proposed formulation with respect to the classical displacement-based and force-based approaches. The influence of the constant axial force criterion will be examined in detail as well as the need for member discretization into several finite elements.

The reference structure is represented by a 3 m steel cantilever column, to which an external constant axial load  $P$  and an incremental lateral displacement  $\Delta$  are applied. The column section (roughly corresponding to an HEA 400 profile) is depicted in Fig. 3(a) as well as the adopted bilinear material constitutive law—Fig. 3(b). The main properties for the material characterization are the steel yield strength ( $f_y=480$  MPa), elastic modulus ( $E_s=200$  GPa), and hardening ratio ( $b=0.005$ ). The coarse sectional discretization adopted, as well as the bilinear steel stress-strain law with post-yield hardening ensure that the computational problem is as simple as possible and avoids numerical problems (such as localization) that may arise with softening behaving materials (e.g. concrete). A high axial load (3500 kN), corresponding to an axial load ratio of 45%, was applied with the aim of better contrasting the results obtained with the different beam element formulations employed.

Force-based (FB), classical displacement-based (DB/c), and axially equilibrated displacement-based (DB/ae) elements are used for the simulation of the member inelastic response. In Fig. 4(a) the results obtained with a single beam element to represent the column are displayed. DB elements featured two Gauss-Legendre integration sections while nine Gauss-Lobatto integration sections were used for the FB element model. As discussed in Calabrese et al. [4], FB elements are sensitive to the element discretization and a minimum number of three IPs is required for good-accuracy solutions with hardening response. DB element models, on the other hand, are only sensitive to the structural discretization and hence it is not justifiable to use more than two Gauss-Legendre integration sections per element [4].

The DB/c element model shows, as expected, a stronger and stiffer response due to the constraints imposed in both the axial and lateral displacement fields. By removing the constraint on the axial displacement field through the iterative procedure introduced in Section 2, the DB/ae becomes considerably softer, yielding a reduction in the simulated lateral strength. However, it can be noted that the latter is still overestimated when compared with the solution provided by the FB formulation, where no displacement fields are assigned and exact equilibrium is

satisfied. Multiple DB elements are required to output a force-displacement response closer to that given by the FB model. This is shown in Figure 4(b), where results from models employing one, two and four DB elements are displayed. Even though mesh refinement leads both DB approaches to nearly match the FB solution, it is evident that the DB/ae element model converges much faster than the one using classical displacement shape functions. Indeed, two DB/ae elements provide a sufficiently accurate solution, which can only be reached with four DB/c.

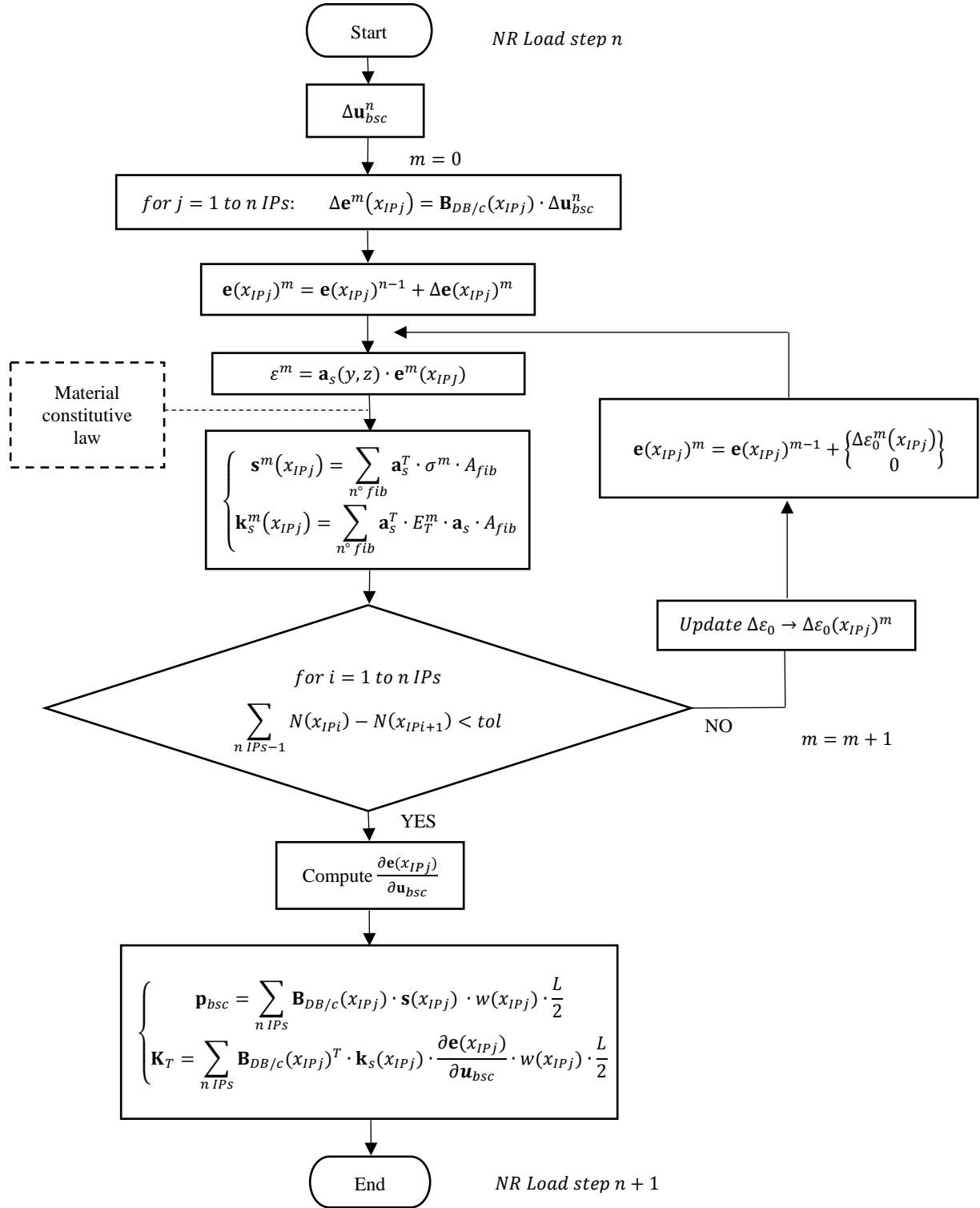


Fig. 2 – Procedure for the element state determination of the axially equilibrated displacement-based element.

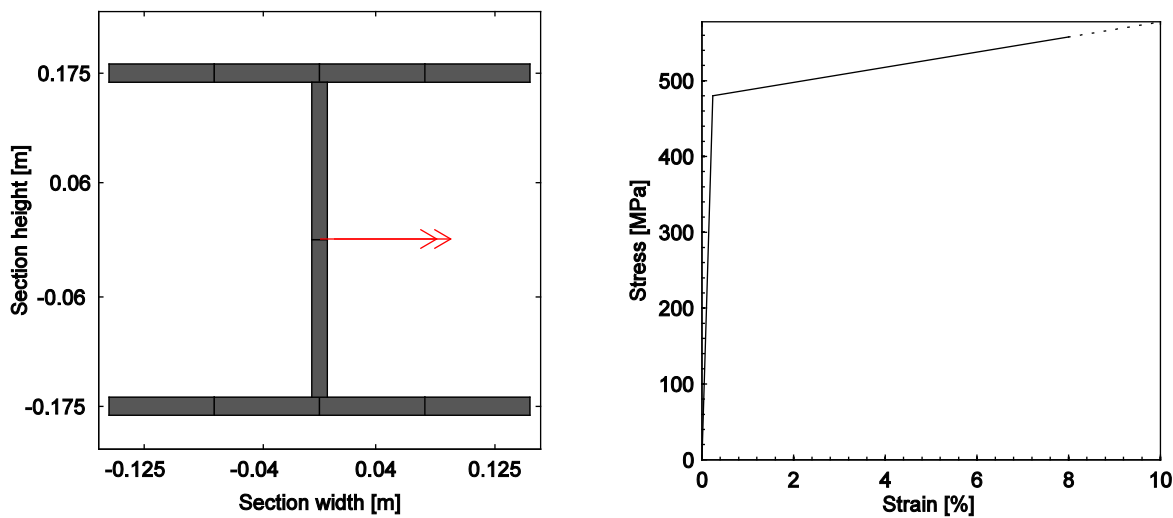


Fig. 3 – Steel column fibre section: (a) Sectional discretization; (b) Steel stress-strain law.

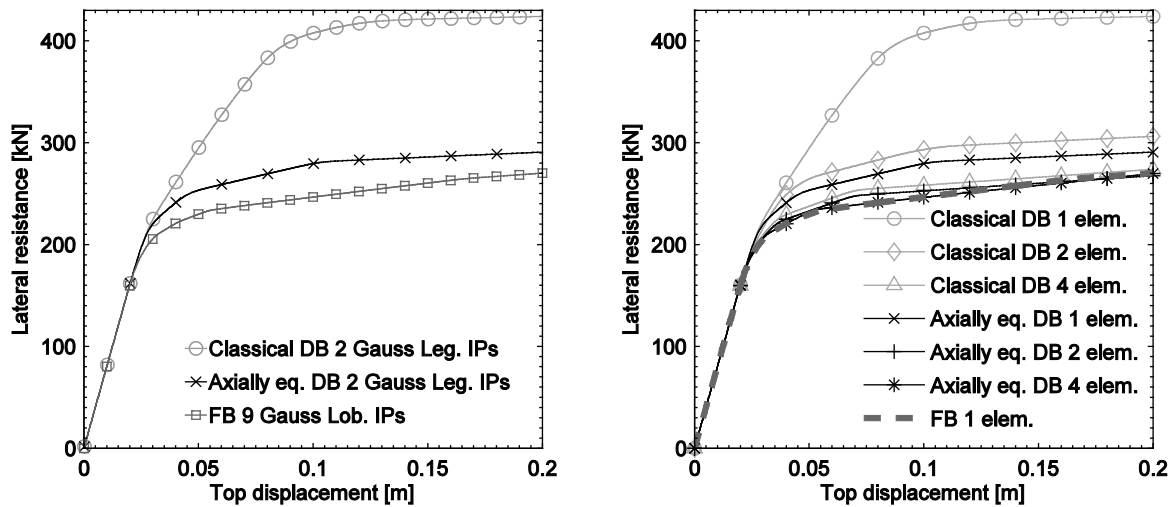


Fig. 4 – Force-displacement response of the steel column: (a) using one element per member; (b) influence of structural member discretization.

The evolution of the axial force during the analyses is shown in Fig. 5(a) at the two integration sections for both the DB/c and DB/ae formulations (the structural member was discretized with only one finite element). As it can be observed, after an initial elastic phase, which ends at around load step 150, the linear axial displacement shape function used in the DB/c element leads to different axial force values in the two integration sections. Although the average axial equilibrium is conserved and hence the average compression force is equal to the applied load  $P$ , the axial force at the bottom and top IPs is symmetric around the mean  $P$ , i.e. it takes a value of  $P \pm \Delta P$ . This inevitably results in a wrong evaluation of the moment capacity for the structural member and therefore of its lateral resistance, which is further enhanced by the inadequate assumption of linear variation of curvatures. On the contrary, the axial force in both IPs of the DB/ae is constant (i.e., axial equilibrium is strictly verified) and always equal to the external applied axial load, thus providing a better estimate of the element moment capacity. Additionally, Fig. 5 (b) displays the good performance of the iterative procedure in terms of the number of global Newton-Raphson iterations required to achieve convergence, which confirms the consistency of the derived element tangent stiffness matrix. However, it has to be recalled that the DB/ae

element requires an additional set of internal iterations at each load step in order to reach the same value of the axial force  $N$  in all integration sections. This extra iteration loop, which complicates the computational process, is not included in classical displacement-based formulations.

Finally, in Fig. 6 the axial strain profiles for the DB/c and DB/ae are shown for different levels of drift. Due to the imposed linear axial displacement field, the axial strain profile for the DB/c is constant. As expected, on account of the shifting of the neutral axis towards the compression side of the section, positive strain values (tension) increasing with the drift demand are observed. On the other hand, the DB/ae shows different strain values in the distinct integration sections, which are the result of the iterative procedure to obtain a constant axial force along the column. The higher tensile average strains are always recorded at the bottom IP. This response better simulates reality than the DB/c element since the shifting of the neutral axis occurs at the cantilever base, where the moment is maximum, rather than along its entire height.

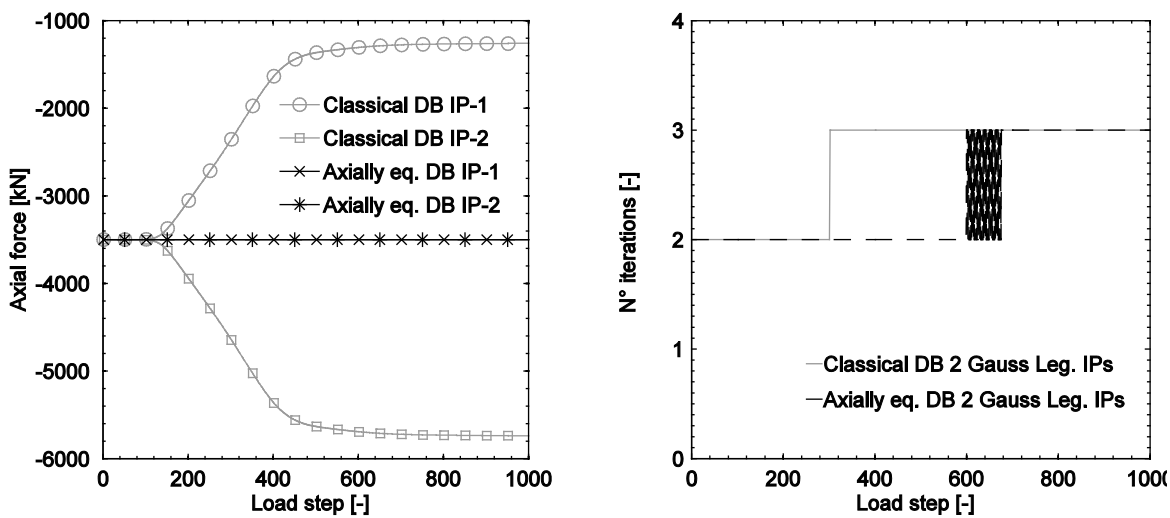


Fig. 5 – (a) Axial force evolution; (b) Number of Newton-Raphson iterations per load step.

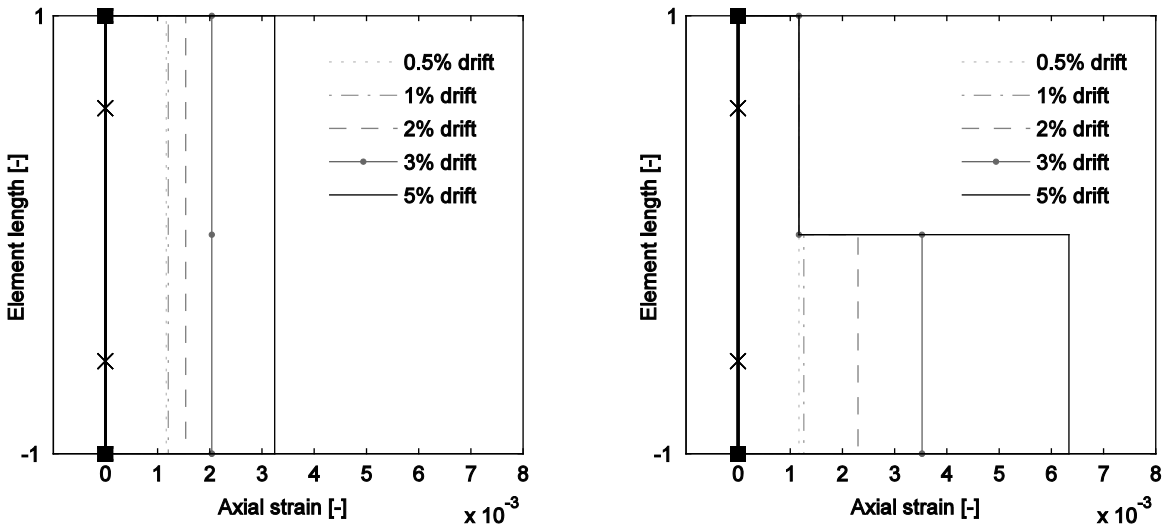


Fig. 6 – Average axial strain profiles at different levels of drift: (a) Classical DB element; (b) Axially equilibrated DB element.

## 4. Validation against Experimental Results

In this section the accuracy of the proposed axially equilibrated displacement-based element (DB/ae) is validated against a quasi-static cyclic test on a circular RC bridge pier performed by Goodnight et al. [10]. The experimental results are compared, both in terms of global (force-displacement) and local (curvature profiles and strain histories) quantities, for models employing DB/ae, DB/c and FB elements.

The cantilever column chosen for the validation is the column T24; it has a nominal diameter of  $D=18$  inches (0.45 m) and a shear span of  $L=156$  inches (3.96 m), corresponding to a shear span ratio  $L/D=8.67$ . The flexural reinforcement consisted of 10 #6 rebars ( $\approx\varnothing19$ mm) while the confinement was provided by a #3 ( $\approx\varnothing10$ mm) spiral at 2 inches ( $\approx50$  mm) pitch. A constant vertical load of roughly 650 kN (corresponding to an axial load ratio of  $N/(f'_c \times A_g) = 10\%$ ) was applied at the column top. The column was subjected to cyclic displacement history with three cycles per displacement amplitude. Target markers attached to the longitudinal rebars in the plastic hinge region allowed on the one hand to continuously track the variation of the local quantities (strains) during the test, and on the other hand to isolate the different contributions to the total lateral displacement (namely displacement due to base rotation and flexural displacement). This is relevant since the FE models used in this study did not account for deformations due to strain penetration into the foundation, which proved to play an important role.

The beam element models used to simulate the experimental results are summarized in Fig. 7(a). Two models constituted by a single FB element were considered, featuring three and five Gauss-Lobatto integration sections. The former represents the minimum number of IPs to simulate the linear response with a FB beam column element without under-integration [4]. However, as discussed before, not less than four IPs should be used for a nonlinear hardening response of a structural member. Despite such consideration, in the present case-study a discretization with three IPs ensured that the influence length of the bottom integration point is similar to the equivalent plastic hinge length as calculated following the expression proposed by [5]. The fulfillment of this condition is recommended to optimize the agreement between the numerical (for FB elements) and the experimental results at the local level [1]. The classical and axially equilibrated displacement-based formulations were also employed: for both cases, models featuring one and two finite elements per structural member were selected. Four Gauss-Lobatto integration sections were used within each DB element for two reasons: (i) the Gauss-Lobatto quadrature rule allows to have an integration section at the element ends, which is useful if base curvatures are to be compared; (ii) although the DB/c formulation is insensitive to element discretization [4], this is less the case for DB/ae elements. However, it could be seen that four IPs are typically sufficient. For the cases where the structural member is discretized with two finite elements, the length of the base element is selected as the upper bound of the measured spread of plasticity, which is given by the following equation [12]:

$$L_{pr} = 2kL + 0.75D$$

where  $L_{pr}$  represents the length of the plastic region,  $k=0.2 \times f_u / f_y - 1 < 0.08$  is the factor accounting for strain penetration as suggested by [5],  $L$  is the shear span, and  $D$  is the column diameter. The same sectional discretization is used for all the models, consisting of 80 confined concrete and 10 steel fibres. No cover concrete was present in the plastic hinge region of test specimen T24 and therefore no unconfined concrete fibres are present in the model.

Fig. 8 depicts the comparison between the experimental and the numerical force-displacement response for all the models discussed above. A different graph is provided for each type of element formulation. Flexural displacements (computed by subtracting the displacement due to base rotation from the total displacement) are reported on the bottom x-axis. The displacement ductility on the top x-axis refers instead to the total lateral displacement because it is the one used in the original reference to identify the imposed demands of the cyclic loading protocol.

Comparing the numerical and experimental global force-displacement curves, one can observe the following points (Fig. 8): (i) The FB models match satisfactorily the experimental data, with the model FB-3IPs slightly underestimating the actual response. This is not surprising since, as discussed in [4], FB elements are characterized by a bottom-up type of convergence, at least in case of hardening response (such as the present

one); (ii) Both DB models using a single element overestimate the experimental F-Δ curve, although the error associated to the DB/ae formulation is sensibly lower than the one of the DB/c. (iii) A good match is obtained by using two DB elements per member, both for the DB/c and the DB/ae.

Model	N° elements	N° IPs*
<b>FB 3 IP</b>	1	3
<b>FB 5 IP</b>	1	5
<b>DB/c 1 ele.</b>	1	4
<b>DB/c 2 ele.</b>	2	4
<b>DB/ae 1 ele</b>	1	4
<b>DB/ae 2 ele.</b>	2	4

\* Gauss-Lobatto quadrature rule

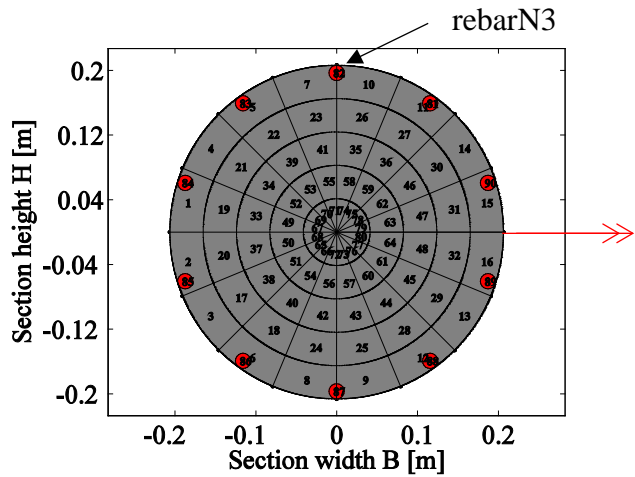


Fig. 7 – (a) Features of the numerical models to simulate unit T24 response; (b) Sectional discretization.

Table 1 – Main material properties used in the numerical models. The material properties are based on the properties reported by Goodnight et al. [10].

Reinforcing steel				Concrete				
$f_y$ [MPa]	$f_u$ [MPa]	$E_s$ [MPa]	b [-]	$f_c$ [MPa]	$f_{cc}$ [MPa]	$E_c$ [MPa]	$\epsilon_c$ [-]	$\epsilon_{cc}$ [-]
470	637	188000	0.0075	44.6	65.6	30000	0.002	0.0067

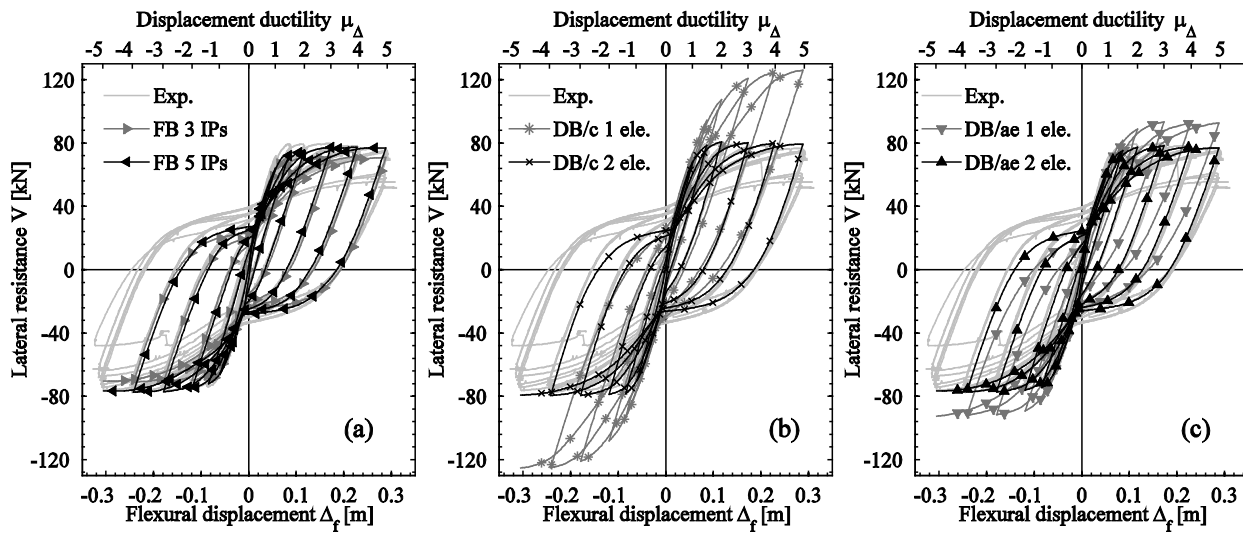


Fig. 8 – Experimental vs numerical force-displacement response: (a) Force-based; (b) Classical displacement-based; (c) Axially equilibrated displacement-based.

Due to the better performance at the global level, the DB/c and DB/ae with 2 elements per member and the FB-5IP will be used for the next comparison at the local level. The experimental and numerical curvature profiles for different levels of displacement ductility are depicted in Fig. 9. At the local level, the better performance of the DB/ae formulation becomes evident: (a) The model FB-5IPs tends to overestimate the actual curvature profiles, and markedly for large drift levels. As an example, the relative error corresponding to the base curvature ( $\eta_{\phi b}$ ) for a ductility demand  $\mu_{\Delta}=5$  is approximately 70%; (b) The opposite trend can be seen for the model employing DB/c elements, which underestimates the real curvature profile ( $\eta_{\phi b}=35\%$  for  $\mu_{\Delta}=5$ ). Moreover, when such elements are employed, it is worthy to notice how the numerical curvature profiles are not continuous along the member length, which is a consequence of the fact that equilibrium is not strictly verified along each finite element; (c) The match between observed and calculated curvature profiles is remarkably improved when DB/ae are used, showing relative errors for the base curvature smaller than 5% for all considered ductility levels.

Finally, as a further local level investigation, the comparison between the experimental vertical strains of rebar N3 (indicated in Fig. 7(b)) monitored at the bottom of the RC column, and the numerical ones (measured at the bottom IP), are shown in Fig. 10. Again, the DB/ae model offers clearly the best agreement between simulation and test data, especially regarding the tensile peak strain levels. An underestimation of the residual strains at zero displacement level is instead common to all three models, indicating that the accumulation of plastic reinforcement strains over multiple cycles is not well captured. However, this issue is not directly related to the element formulation and could arguably be addressed with more advanced steel and concrete constitutive relationships.

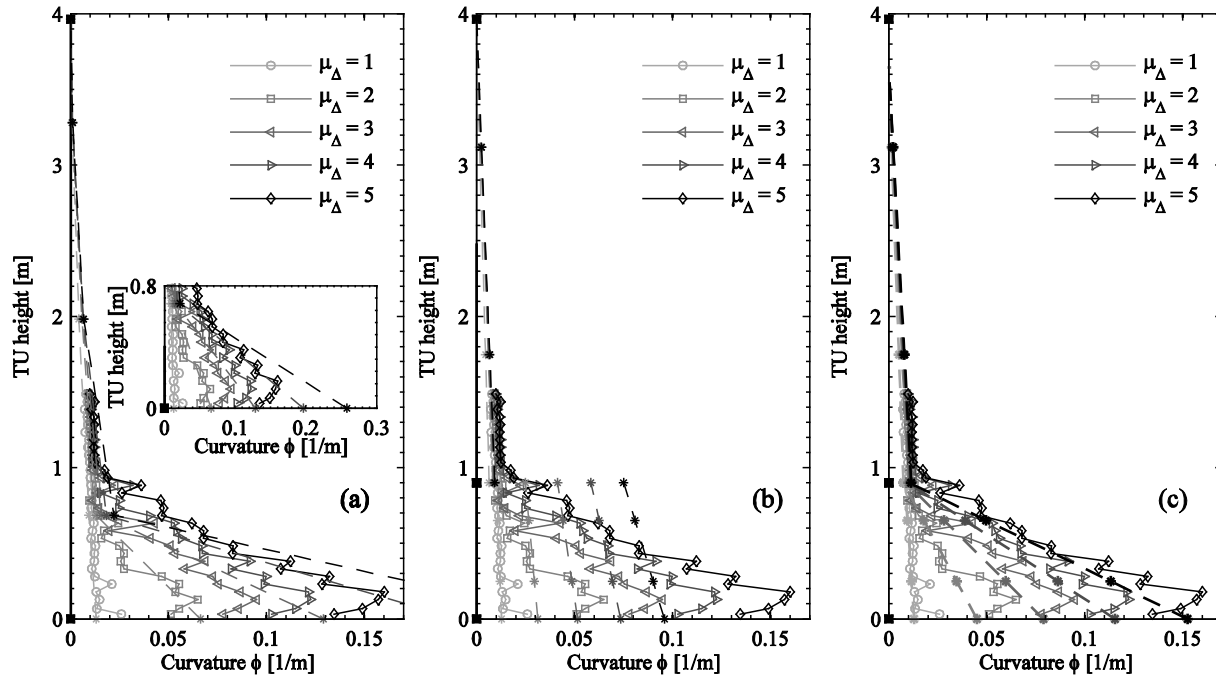


Fig. 9 – Experimental vs numerical curvature profiles: (a) Force-based; (b) Classical displacement-based; (c) Axially equilibrated displacement-based.

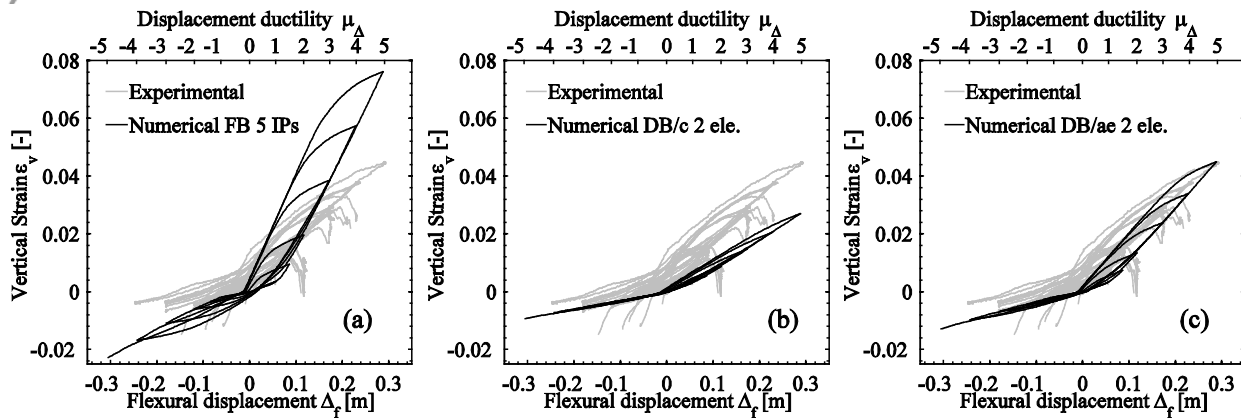


Fig. 10 – Experimental vs numerical strain histories at the base of rebar N3: (a) Force-based; (b) Classical displacement-based; (c) Axially equilibrated displacement-based.

## 5. Conclusions and Future Work

The linear shape functions used to describe the axial displacement field in classical displacement-based formulations constitute a significant limitation in the accuracy of this finite element approach when inelastic material behaviour is considered. The resulting axial forces become equilibrated only in an average sense, inevitably leading to a poor local and global performance of the finite element.

In this paper a displacement-based element strictly satisfying axial equilibrium is presented. The pointwise equilibrium is achieved by an additional intra-element iterative procedure that automatically recalculates the axial strain profile required to guarantee such axial force equilibrium. Once the latter condition is met, the principle of virtual work is employed to compute the element basic forces and to obtain a consistent stiffness matrix.

An application example is used to compare the element formulation described above against classical displacement-based and force-based approaches. The strengths and weaknesses of the proposed formulation are pinpointed both at the global and local level. Namely, it is shown that when compared with the classical displacement-based approach, a more exact solution can be obtained both in terms of force-displacement response and average axial strain profiles along the member length. These improved simulations do not come at the expense of relevant additional computational time.

The axially equilibrated displacement-based element is then used to model a cyclic test on a RC cantilever column. Assuming an appropriate member discretization, it provides encouraging results both in terms of global and local level responses. Namely, the simulation of curvature profiles and strain histories compares particularly well with experimental results, especially if contrasted with models using classical force-based or displacement-based elements.

The element presented herein is intended as a first step in the formulation of a more sophisticated beam element. The latter will include, among others, the modification of the imposed transversal displacement profile in order to account for physically relevant effects in the nonlinear cyclic response of RC members, such as the evolution of the plastic hinge length with increasing ductility demands.

## Acknowledgments

The financial support provided by the Office Fédéral des Routes (OFROU) is kindly appreciated.

## References

- [1] J.P. Almeida, D. Tarquini, K. Beyer, Modelling approaches for inelastic behaviour of RC walls: Multi-level

- assessment and dependability of results, *Arch. Comput. Methods Eng.* 23 (2016) 69–100.
- [2] SeismoSoft, SeismoStruct - A Computer Program for Static and Dynamic Nonlinear Analysis of Framed Structures, (2013).
- [3] F. McKenna, G.L. Fenves, M.H. Scott, B. Jeremic, Open System for Earthquake Engineering Simulation (OpenSees), Berkeley, California, U.S.A., 2000.
- [4] A. Calabrese, J.P. Almeida, R. Pinho, Numerical issues in distributed inelasticity modeling of RC frame elements for seismic analysis, *J. Earthq. Eng.* 14 (2010) 38–68. doi:10.1080/13632469.2010.495681.
- [5] M.J.N. Priestley, G.M. Calvi, M.J. Kowalsky, Displacement-based seismic design of structures, IUSS Press, 2007.
- [6] E.M. Hines, Seismic Performance of Hollow Rectangular Reinforced Concrete Bridge Piers with Confined Corner Elements, 2002.
- [7] Y.D. Hose, F. Seible, M.J.N. Priestley, Strategic Relocation of Plastic Hinges in Bridge Columns, San Diego, California, 1997.
- [8] Y.H. Chai, M.J.N. Priestley, F. Seible, Flexural retrofit of circular reinforced concrete bridge columns by steel jacketing: experimental studies, *Struct. Syst. Res. Proj.* 91/06, Univ. Calif. (1991) 151.
- [9] J.C. Goodnight, M.J. Kowalsky, J.M. Nau, A new look at strain limits and plastic hinge lengths for reinforced concrete bridge columns, in: 10th U.S. Natl. Conf. Earthq. Eng., Anchorage, 2014.
- [10] J.C. Goodnight, M.J. Kowalsky, J.M. Nau, Effect of Load History on Performance Limit States of Circular Bridge Columns, *J. Bridg. Eng.* 18 (2013) 1383–1396. doi:10.1061/(ASCE)BE.1943-5592.0000495.
- [11] B. Izzuddin, C. Karayannis, A. Elnashai, Advanced nonlinear formulation for reinforced concrete beam-columns, *J. Struct. Eng.* 120 (1994) 2913–2934.
- [12] J.C. Goodnight, Y. Feng, M.J. Kowalsky, J.M. Nau, The Effects of Load History and Design Variables on Performance Limit States of Circular Bridge Columns. Volume 1, 4000 (2015).